



Research article

Investigating the effects of *Laggera pterodonta* on H3N2-Induced inflammatory and immune responses through network pharmacology, molecular docking, and experimental validation in a mice model

Yaorong Chen^{a,b,1}, Zexing Chen^{a,b,1}, Wanqi Wang^{a,b,1}, Yutao Wang^a, Jinyi Zhu^{a,b}, Xinhua Wang^{a,b,**}, Wanyi Huang^{a,b,*}

^a State Key Laboratory of Respiratory Disease, National Clinical Research Center for Respiratory Disease, Guangzhou Institute of Respiratory Health, The First Affiliated Hospital of Guangzhou Medical University, Guangzhou, 510180, China

^b Institute of Integration of Traditional and Western Medicine, The First Affiliated Hospital of Guangzhou Medical University, Guangzhou, China

ARTICLE INFO

Keywords:

Laggera pterodonta
Influenza A/Aichi/2/1968 virus (H3N2)
Network pharmacology
Molecular docking
Inflammation
Immunity

ABSTRACT

For centuries, *Laggera pterodonta* (LP), a Chinese herbal medicine, has been widely employed for treating respiratory infectious diseases; however, the mechanism underlying LP's effectiveness against the influenza A/Aichi/2/1968 virus (H3N2) remains elusive. This study aims to shed light on the mechanism by which LP combats influenza in H3N2-infected mice. First, we conducted quasi-targeted metabolomics analysis using liquid chromatography-mass spectrometry to identify LP components. Subsequently, network pharmacology, molecular docking, and simulation were conducted to screen candidate targets associated with AKT and NF- κ B. In addition, we conducted a series of experiments including qPCR, hematoxylin-eosin staining, flow cytometry, immunohistochemistry, and enzyme-linked immunosorbent assay to provide evidence that LP treatment in H3N2-infected mice can reduce pro-inflammatory cytokine levels (TNF- α , IL-6, IL-1 β , and MCP-1) while increasing T cells (CD3⁺, CD4⁺, and CD8⁺) and syndecan-1 and secretory IgA expression. This, in turn, aids in the prevention of excessive inflammation and the fortification of immunity, both of which are compromised by H3N2. Finally, we utilized a Western blot assay to confirm that LP indeed inhibits the AKT/NF- κ B signaling cascade. Thus, the efficacy of LP serves as a cornerstone in establishing a theoretical foundation for influenza treatment.

Abbreviations: LP, *Laggera Pterodonta*; H3N2, influenza A/Aichi/2/1968 virus; LC-MS/MS, Liquid chromatography mass spectrometry; qPCR, quantitative real-time polymerase chain reaction; GO, Gene Ontology; KEGG, Kyoto Encyclopedia of Genes and Genomes; PPI, Protein-Protein Interaction network; MDCK, Madin-Darby canine kidney; ELISA, enzyme-linked immunosorbent assay; HE, Hematoxylin and eosin; OMIM, Online Mendelian Inheritance in Man; IHC, Immunohistochemical; FBS, fetal bovine serum.

* Corresponding author. Department of Traditional Chinese Medicine, The First Affiliated Hospital of Guangzhou Medical University, Guangzhou, 510120, China.

** Corresponding author. State Key Laboratory of Respiratory Disease, National Clinical Research Center for Respiratory Disease, Guangzhou Institute of Respiratory Health, The First Affiliated Hospital of Guangzhou Medical University, Guangzhou, 510180, China.

E-mail addresses: xinhuaw@gzhmu.edu.cn (X. Wang), 13724161240@163.com (W. Huang).

¹ Equal contributors.

<https://doi.org/10.1016/j.heliyon.2024.e29487>

Received 12 October 2023; Received in revised form 8 April 2024; Accepted 8 April 2024

Available online 10 April 2024

2405-8440/© 2024 The Authors. Published by Elsevier Ltd. This is an open access article under the CC BY-NC-ND license (<http://creativecommons.org/licenses/by-nc-nd/4.0/>).

1. Introduction

Globally, influenza—a highly contagious acute respiratory disease—has significantly affected human health, leading to 1 billion infections, of which 3–5 million are associated with severe illness and 300,000–500,000 with fatalities [1]. This not only threatens global public health security but also imposes a substantial economic burden on society. Influenza is caused by influenza A and B in humans. Notably, the influenza A virus H3N2 subtype is associated with increased rates of intensive care unit admissions due to influenza, compared with the H1N1 subtype and influenza B virus [2]. Infected individuals typically manifest symptoms such as fever, cough, runny nose, sore throat, and fatigue; in severe cases, life-threatening pneumonia may occur, especially prevalent among children and the elderly [3]. However, due to the frequent antigenic mutations of the influenza virus, current vaccines, and antiviral drugs, such as M2 inhibitor adamantane and NA inhibitor oseltamivir, have proven ineffective in timely reducing the risk of widespread influenza outbreaks [4–6]. Consequently, it is critical to find and create more efficient remedies.

According to traditional Chinese medicine theory, influenza, as a seasonal epidemic, falls under the category of “plague” within the ancient Chinese science of warm diseases. Traditional Chinese herbal medicines have been employed for many years to treat influenza. Moreover, *in vitro* and *in vivo* experiments have demonstrated that these herbal remedies can directly reduce viral replication and indirectly inhibit viral invasion or replication by controlling the immune system and inflammatory response of the body [7]. Currently, numerous research endeavors have embarked on exploring the pharmaceutical effects against influenza of compounds derived from traditional herbal medicines. For instance, like *Coptis chinensis* Franch. and *Phellodendron chinense* Schneid., among others, has demonstrated the ability to alleviate inflammatory lesions induced by the influenza virus by restricting NLRP3 inflammasome activation [8]. Paeoniflorin, isolated from *Paeonia lactiflora* Pall, has been demonstrated to protect against IAV-induced acute lung injury by blocking the $\alpha\beta3$ /TGF- $\beta1$ pathway [9]. Therefore, it is deemed reliable to explore potential compounds extracted from traditional Chinese herbal medicines with a history of influenza treatment.

Laggera pterodonta (LP), a perennial herbaceous plant widely found in Yunnan Province, China, is a traditional Chinese herbal medicine employed for diseases such as colds, coughs, bronchitis, and other respiratory tract infections for centuries [10]. Current pharmaceutical research has revealed that several compounds extracted from LP possess antiviral, anti-inflammatory, antioxidant, and acetylcholinesterase inhibitory properties [11–13]. For instance, pterodontic acid has demonstrated the ability to inhibit influenza virus replication and reduce inflammation *in vitro* [14]. However, monomer compounds in LP may extend beyond those mentioned earlier, and there are potentially more noteworthy compounds within LP worth exploring. Hence, this study employed quasi-targeted metabolomics analysis using liquid chromatography-mass spectrometry (LC-MS/MS) [15], which identified 1600 compounds within LP. Given the thousands of compounds present in LP, investigating the pharmaceutical effects and mechanisms of these compounds for treating influenza without utilizing bioinformatics analysis, including network pharmacology, molecular docking, and simulation [16, 17], would be an immense drain on resources, time, and the economy. Moreover, there remains a lack of clarity regarding LP's activity against H3N2 and the *in vivo* molecular mechanisms.

In this study, by integrating data from the LC-MS/MS analysis, PubChem database, Swiss Target database, TargetNet database, Gene Cards, and the Online Mendelian Inheritance in Man (OMIM) database, we constructed a pharmacological network of LP's targets against influenza. Additionally, to predict hub genes, we employed protein-protein interaction (PPI) network analysis, Gene Ontology (GO), and Kyoto Encyclopedia of Genes and Genomes (KEGG) pathway enrichment, and molecular docking and simulation. Subsequently, we conducted *in vivo* experiments to identify the target genes and the underlying mechanism of action of LP in controlling inflammation and immunity against H3N2.

2. Methods and materials

2.1. Preparation and analysis of LP extract

The aerial parts of LP (5 kg) were collected in November 2022 from Yunnan, China. Each collected sample was stored at the College of Pharmaceutical Sciences (Kunming Medical University, Kunming, China) with voucher specimen (NO. 220920) after validation by Professor Rongping Zhang (College of Pharmaceutical Sciences; Kunming Medical University). Thereafter, 300 g of the samples was cleaned and soaked in 4 L of distilled water, followed by a 15-min decoction. Subsequently, the resulting supernatant underwent freeze-drying, yielding 10 g of powder, which was securely sealed in a medicine cabinet.

Initially, 100 μg samples were introduced into EP tubes and resuspended in prechilled 80 % methanol through vigorous vortexing. After incubation on ice for 5 min, the suspended samples underwent centrifugation at 15,000 g, 4 °C for 20 min. Upon the removal of sediment, the supernatant was diluted to a final concentration of 53 % with LC-MS grade water. Processed samples were relocated to a fresh EP tube and subjected to another round of centrifugation at 15,000 g, 4 °C for 20 min. The resultant supernatant was introduced into the LC-MS/MS system and analyzed on the ExionLC™ AD system (SCIEX) coupled with the QTRAP® 6500+ mass spectrometer

Table 1

The solvent gradient with the Xselect HSS T3 column.

Step	Time/min	Eluent A (0.1 % Formic acid water)	Eluent B (0.1 % Formic acid-acetonitrile)
1	0–15	98 %	2 %
2	15–17	0 %	100 %
3	17.1–20	98 %	2 %

(SCIEX) at Novogene Co., Ltd. (Beijing, China). The Xselect HSS T3 column (2.1×150 mm, $2.5 \mu\text{m}$; Waters, USA) was utilized for sample analysis, employing a 20-min linear gradient at a flow rate of 0.4 mL/min for both positive and negative polarity modes. Eluent A (0.1% formic acid-water) and B (0.1% formic acid-acetonitrile) were the solvents employed, and the details of the solvent gradient can be found in Table 1 [18]. The QTRAP® 6500+ mass spectrometer functioned in both positive (curtain gas: 35 psi, collision gas of medium, ion spray voltage: 5500V, temperature: $550 \text{ }^\circ\text{C}$, ion source gas 1: 60, ion source gas 2: 60) and negative (curtain gas: 35 psi, collision gas of medium, ion spray voltage of -4500V , temperature: $550 \text{ }^\circ\text{C}$, ion source gas 1: 60, ion source gas 2: 60) polarity modes. For metabolite detection, the SCIEX QTRAP 6500+ mass spectrometer operated in the multiple reaction monitoring mode. Quantification of compounds was based on Q3 (daughter ion), with qualitative analysis relying on retention time, daughter ion pairs (Q1/Q3), declustering potential, collision energy, and the secondary spectral data of the detected substances [19,20].

2.2. Network pharmacology

2.2.1. Collection of chemical compounds of LP and construction of the PPI network of common targets of LP and influenza

LC-MS/MS results for targeted metabolism were used to calculate the relative peak area values using the SCIEX OS software (Version 1.4). The top 10 natural compounds with a CAS number from LP that displayed high peak area values were selected to identify potential targets. We retrieved the Simplified Molecular Input Line Entry System (SMILES) formats of the compounds from the PubChem database (<https://pubchem.ncbi.nlm.nih.gov>) and incorporated into the TargetNet (<http://targetnet.scbdd.com>) and the Swiss Target (<https://cn.string-db.org/>) databases. In the TargetNet database, we specifically chose targets with a probability value > 0 , which meant the compounds had the potential to act on the targets. In Swiss Target Prediction, we selected the top 15 targets with a probability value > 0.1 . Subsequently, we combined the targets obtained from both databases, removing any duplicate entries. Furthermore, to identify influenza-related targets, a search using the term “Influenza” was conducted in two additional databases: the Gene Cards (<https://www.genecards.org/>) and OMIM database (<https://www.omim.org/>). Thereafter, to visualize the interaction targets of LP and influenza, we uploaded the prospective targets and disease targets to the Venny 2.1 platform (<https://bioinfo.cnb.csic.es/tools/venny/index.html>). We also imported these targets into STRING, selected “*Homo sapiens*” proteins, and set a medium interaction score of 0.400 (a score < 0.4 indicates relatively low target linkage), to elucidate the biological significance of the shared targets. Finally, we constructed the PPI network using Cytoscape software, version 3.7.2.

2.2.2. Pathway enrichment analysis

We employed DAVID (<https://david.ncicfcrf.gov>) for functional GO and KEGG pathway enrichment, aiming to identify the predicted targets.

2.3. Molecular docking and molecular dynamics simulation

PI3K (Protein Data Bank ID: $2 \times 6\text{K}$), AKT (Protein Data Bank ID: 2GU8), TNF (Protein Data Bank ID: 6×81), and NF- κB -P65 (Protein Data Bank ID: 7BIY) were chosen as the receptors for interaction with the top 10 natural compounds exhibiting high expression within LP. The ligands' structural files in MOL2 format were acquired from PubChem (<https://pubchem.ncbi.nlm.nih.gov>). Each compound was introduced into Autodock Tools software 1.5.6 as a ligand, facilitating docking with the respective targets to generate docking scores and determine active sites of the proteins [21]. Discovery Studio 2019 (BIOVIA) software was used for 2D and 3D visualizations and analysis of the docked complexes [22]. A 100-ns molecular dynamics simulation was performed using YASARA STRUCTURE version 20.7.4.W.64, employing the AMBER14 force field [23] and the TIP3P solvation model [24]. Following the refinement of the complexes, a simulation cell with periodic boundary conditions (298 K , $\text{pH } 7.4$, 0.9% NaCl) was established. Simulated annealing was implemented with a time step of 2.0 fs , and long-range electrostatic interactions (cutoff radius: 8.0 \AA) were determined using the Particle Mesh Ewald algorithm [25]. Trajectories were sampled at intervals of 100 ps over 100 ns , and a comprehensive analysis table, encompassing the root-mean-square deviation (RMSD) versus time plot, was generated within the YASARA interface.

2.4. Docking validation and comparison methodology

The native ligands were re-docked to the targeted proteins, and the RMSD was calculated to verify the reliability of the docking methodology. Subsequently, known target protein inhibitors reported previously were subjected to molecular docking using the same protocol, and their interactions were visualized with Discovery Studio 2019 (BIOVIA) software.

2.5. Study on animals

2.5.1. Preparation of the animal models

We procured 6–8 weeks old BALB/c mice weighing between 16 and 18 g from Charles River Animal Technology Co., Ltd. (Zhejiang, China). The mice were granted food and water ad libitum, housed in controlled environmental conditions (temperature: $22 \pm 1 \text{ }^\circ\text{C}$, relative humidity: $55 \pm 10 \%$), and maintained on a 12-h light/dark cycle. They were kept in a facility that adhered to specific pathogen-free standards. All research procedures adhered to the rules outlined by the Laboratory Animal Center of Guangzhou Medical University and complied with animal protection legislation. The study received approval from the Guangzhou Medical University Animal Care and Use Committee (2022350).

To ascertain the median lethal dose (LD50) of the influenza A/Aichi/2/1968 virus (H3N2) in mice ($n = 10$ in each group), the mice were randomly categorized into eight groups. One control group and seven experimental groups with 10-fold dilutions of viruses were included in these groupings (10^{-1} , 10^{-2} , 10^{-3} , ... 10^{-7}). After being conducted under light isoflurane anesthesia, the control group received 50- μ L PBS intranasally, while treated groups received the same volume of PBS containing varying titers of H3N2. Thereafter, daily monitoring of the mice was conducted for up to 15 days post-infection, with their survival and body weight recorded once each day. According to Chinese animal protection laws, any mouse that experienced weight loss exceeding 20 % of its original weight was considered deceased. The LD50 values ($10^{-1.67}$ TCID₅₀) were calculated using the Reed-Muench method and results are present in Table 2. We selected an LD50 dose to infect the mice in the formal experiments. In addition, the toxicity of the BALB/C mice with LP oral administration have been conducted for 14 d. According to the OECD Guideline No.425: Up-and-Down Procedure [26], three different doses of LP powder extracted before and dissolved in PBS were administrated to the mice as follows: 2.4, 1.2, and 0.6 g/kg. The body weight, mortality, and the signs of toxicity (i.e., tremors, convulsions, salivation) of mice were evaluated. And there were no any obviously abnormal change of mice and LD50 of LP was >2 g/kg. Therefore, the two concentrations of LP (0.6 and 1.2 g/kg) were chosen in our subsequent experiments.

In the formal experimental phase, a new set of mice was randomly allocated to five groups ($n = 8$ per group): normal control (Ctrl), virus (H3N2), virus (H3N2) plus oseltamivir 60 mg/kg (OSE), virus (H3N2) plus high-dose LP (LP 1.2 g/kg), and virus (H3N2) plus low-dose LP (LP 0.6 g/kg). Each of the mice in the Ctrl group received intranasal administration of 50 μ L of PBS, whereas those in the infected groups received intranasal administration of 50 μ L of H3N2 ($10^{-1.67}$ TCID₅₀). Oseltamivir and two concentrations of LP were dissolved in PBS. Four hours post-infection, Ctrl and H3N2 mice received oral administration of PBS, while the remaining groups were orally administered the oseltamivir or two concentrations of LP respectively once daily for a duration of 5 days. 24 h after the last treatment mice were anesthetized with isoflurane and then dissected to remove the lungs after decapitation and execution. The lung index was calculated using the following formula: The lung index = The weight of lung of mouse/The body weight of mouse on last day $\times 100$ %.

2.5.2. Detection of viral titers in lung of mice

The lungs from mice were placed in 2-mL EP tubes with 1 mL of PBS. Each tube was equipped with one 4-mm and two 3-mm steel balls, which were subjected to homogenization at 60 Hz for 60 s. Subsequently, the EP tubes were placed for centrifugation at 4 °C, 5000 rpm for 5 min, and the supernatant was collected, partitioned, and stored at -80 °C. Madin-Darby canine kidney (MDCK) cells were obtained from the American Type Culture Collection (USA) and cultured in DMEM/F12 (Gibco, USA) containing 10 % heat-inactivated fetal bovine serum (FBS) and 1 % penicillin-streptomycin. The experiment involved placing MDCK cells (2×10^4 cells/well) in 96-well plates for monolayer formation at 37 °C. The lung homogenate supernatant was added to each well at a volume of 100 μ L, with concentrations replicated in four wells. Additionally, a normal control group was established using an equal amount of DMEM/F12. Following a 2-h incubation, the supernatant was discarded, and wells were washed twice with PBS. Fresh DMEM/F12 was added, and cells were incubated for an additional 48 h. Daily observations were made for cell growth and signs of cellular damage (shrinkage, rounding, and detachment [cytopathic effect or CPE]). The Reed-Muench method was employed to calculate the viral titers [27].

2.5.3. Hematoxylin-eosin (HE) staining of lung tissue

Following a 48-h preservation at room temperature (RT) in a 4 % PBS-paraformaldehyde solution (pH 7.4), the lung tissues of mice in the experiment underwent embedding in paraffin. Subsequent to dehydration and clearing, the tissues were sliced into 4- μ m-thick sections and immersed in wax. Then, these portions were dewaxed and stained with HE. The staining procedure followed established procedures, and fully automated digital slice scanning equipment was used to complete the task (Panoramic C-Scan, Japan) [28].

2.5.4. Flow cytometric analysis of lung tissue

The lungs from the mice after harvesting were mechanically fragmented into small tissue pieces and immersed in a 5-mL solution containing 2 % FBS, 2 mM L-glutamine, 25 mM HEPES in HBSS, 0.1 mg/mL DNase I, and 1 mg/mL collagenase D (Roche, UK). The mixture was then subjected to incubation for 30 min at 37 °C. After dislodging the fragments through a 40- μ m cell strainer (BD Pharmingen, USA), remaining red blood cells were lysed using red blood cell lysis buffer, and the resulting cell pellets were suspended

Table 2
Determination of median lethal dose (LD50) in H3N2 influenza-infected mice.

Virus Dilution	Number of deaths	Number of survivors	Accumulation	Accumulation	Total	Deaths Proportion of	Deaths Percentage
			Number of deaths	Number of survivors			
10^{-1}	9	1	11	1	10	9/1	100
10^{-2}	2	8	2	9	10	2/8	25
10^{-3}	0	10	0	19	19	0	0
10^{-4}	0	10	0	29	29	0	0
10^{-5}	0	10	0	39	39	0	0
10^{-6}	0	10	0	49	49	0	0
10^{-7}	0	10	0	59	59	0	0

in FACS buffer. Fc receptors were blocked using 0.5 mg/mL of anti-mouse CD16/32 (BD Pharmingen, USA), and the cells were examined using anti-mouse antibodies AF700 (BD Pharmingen, USA), FITC anti-mouse CD3, Bv510 anti-mouse CD45, APC anti-mouse CD4 (BD Pharmingen, USA), and BV650 anti-mouse CD8 (BD Pharmingen, USA). Flow cytometry was performed on the BD LSRFortessaX-20 flow cytometer (Becton, Dickinson, and Company, USA), analyzed with FlowJo software [29].

2.5.5. Enzyme-linked immunosorbent assay (ELISA) of lung tissue

Secretory IgA (sIgA) concentrations in the lung homogenate supernatant were quantified using a mouse ELISA kit (CSB-E08413 m, CUSABIO) adhering to the manufacturer's instructions. The ELISA kit was brought to RT for 30 min before use. After previously frozen lung homogenate supernatants were thawed at room temperature, they were loaded into wells, incubated for 2 h at 37 °C, and then subjected to the following steps: biotin-antibody was introduced (additional hour of incubation at 37 °C), five buffer washes, horseradish peroxidase conjugate was added (incubated for another hour at 37 °C), and chromogenic substrate was introduced (incubated for 15 min at 37 °C). Finally, the measurement of absorbance at 450 nm was carried out using a microplate reader (Thermo Fisher Scientific Inc., Waltham, MA, USA) [30].

2.5.6. RNA extraction and quantitative real-time polymerase chain reaction (qPCR) assay of lung tissue

Lung homogenate supernatants were subjected to mRNA extraction utilizing 1 mL of TRIzol (Thermo Fisher, USA). The mixture underwent a 5-min incubation at RT, followed by vigorous shaking with 200 μ L of chloroform for 15 s, a 3 min incubation at RT, and a subsequent 15-min centrifugation at 4 °C. After collecting the supernatant, it was combined with 500 μ L of isopropanol and left to incubate for 10 min at RT. Following a 10-min centrifugation at 4 °C, the supernatant was discarded, and the precipitate was washed with 1 mL of 75 % ethanol. After a 10-min centrifugation at 4 °C, 10,000 rpm, the supernatant was again discarded, and RNA was dissolved in 50 μ L of DEPC water. The quantification and purity assessment of the extracted RNA were performed using the DS-11+ ultra-micro spectrophotometer (DeNovix). For reverse transcription, 1000 ng of total RNA was converted to cDNA using PrimeScriptTM RT Master Mix (Perfect Real Time) from Vazyme Bio, Nanjing, China. The resulting cDNA underwent qPCR using the GeneAmp[®] PCR Instrument 9700 ChamQ Universal SYBR qPCR Master Mix on the ABI 7500 RT-PCR system (Vazyme Bio, China). Relative gene expression levels were normalized to β -actin using the $2^{-\Delta\Delta Ct}$ method. The primer sequences are listed in Table 3 [28].

2.5.7. Immunohistochemical (IHC) examination

For IHC, the processes of fixing, embedding, and sectioning lung tissue mirrored those employed in HE staining. After dewaxing with xylene and undergoing rehydration through an ethanol gradient, the tissue slides underwent a wash with deionized water. Antigenic repair procedures were conducted using a microwave and antigenic repair solutions. Following this, the slides were coated with 10 % bovine serum albumin and left to seal for 30 min at RT. Subsequent to the sealing step, the slides were subjected to incubation with syndecan 1 (SDC-1; Abcam, 1:500 dilution) at 4 °C overnight and then with a secondary antibody at RT for 1 h. Shadowing was accomplished with DAB, and redyeing was performed with hematoxylin. Photomicrographs were captured using the Panoramic MIDI system [28].

2.5.8. Western blot assay

Proteins from lung tissue were extracted by homogenization in RIPA buffer (Solarbio, Beijing, China) with full Mini protease inhibitor cocktail tablets (Sigma, USA). After centrifuging at 12,000 rpm, 4 °C for 15 min, the supernatant was gathered, and protein concentrations were determined using a BCA assay (Thermo Scientific, USA). Following this, equal protein amounts (15 μ g) from each sample were separated on 10 % sodium dodecyl sulfate-polyacrylamide gels and transferred to PVDF membranes, and were blocked with TBST containing 5 % bovine serum albumin for 1 h. Then, specific primary antibodies from Cell Signaling Technology (CST) were used for incubation: anti-AKT (#2920, 1:1000 dilution), anti-NF- κ B-P65 (#8242, 1:1000 dilution), anti-Phospho-AKT (#4060, 1:1000 dilution), anti-Phospho-NF- κ B-P65 (#3033, 1:1000 dilution), anti- β -actin (#4970, 1:1000 dilution). Following this, the membranes were incubated with HRP-conjugated secondary antibodies (#7074 or #7076, 1:5000 dilution) for 1 h at RT, and enhanced chemiluminescence (ECL) blotting tool (BIORAD) was employed to detect antibodies bound to the membranes, and band intensities were quantified with ImageJ software 1.54f (National Institutes of Health, USA) [28].

2.6. Statistical analysis

Data are presented as mean and standard deviation (SD). We employed IBM SPSS Statistics for Windows, version 25.0 (IBM, NY, USA) for statistical analysis. For normally distributed data, one-way analysis of variance before performing Tukey's test was conducted

Table 3
The primers for qPCR.

Gene	Forward sequences	Reverse sequences
IL-1 β	GTGTCITTCCTGGACCTT	TCGTTGCTTGGTTCCTTG
IL-6	AGTTGCCTTCTGGACTGA	GCCACTCCTTCTGTACTCC
TNF- α	ACGTGGAAGTGGCAGAAGAG	CTCCTCCACTTGGTGGTTTG
MCP-1	TTCACCAGCAAGATGATCCCA	TCCTTCTTGGGGTCAGCACA
β -actin	AGAGGGAAATCGTGCGTGAC	CAATAGTGATGACCTGGCCCG

to determine differences among three or more groups. $*p < 0.05$, $**p < 0.01$, and $***p < 0.001$ were indicative of statistical significance.

3. Results

3.1. Construction of PPI network of common targets of LP and influenza

Through LC-MS/MS analysis, 1600 compounds in LP were discovered (Multimedia component 1). From this list, we selected the top natural 10 compounds with the highest expression levels to screen for potential gene targets (refer to Table 4). We identified 396 target genes associated with the compounds of LP using Swiss Target Prediction and TargetNet. Additionally, we found 1456 target genes associated with influenza in both Gene Cards and OMIM databases. 86 target genes were common to both influenza viruses and the compounds of LP (as shown in Fig. 1A). Common targets were entered into STRING to obtain information about shared potential targets. Subsequently, the STRING-derived data were imported into Cytoscape to build a PPI network made up of 83 nodes and 895 edges (Fig. 1B). A higher node degree indicates a greater likelihood of eliciting an effect through the respective target. The top 5 nodes with the highest degree obtained in this study were TNF, AKT1, STAT3, GAPDH, and SRC. Notably, the average node degree stood at 21.6, with 38 targets surpassing this average.

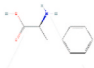
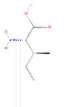
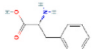
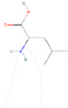
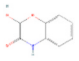
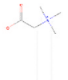
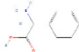
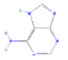
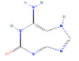
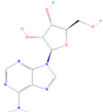
3.2. Analysis of GO functional and KEGG pathway enrichment

To determine the modes of action of the compounds, we conducted GO functional and KEGG pathway enrichment analyses. Terms with $p < 0.05$, minimum count of 3, and enrichment factor >1.5 (ratio of observed counts to counts expected by chance) were collected. Subsequently, these terms were categorized into clusters based on their shared memberships. The top three biological processes identified, with the lowest p -values, were positive control of cytokine production, reaction to lipopolysaccharide and response to molecule of bacterial origin (Fig. 2A). The top three cellular components were membrane raft, membrane microdomain and vesicle lumen (Fig. 2A). The top three identified molecular functions were protein serine kinase activity, protein serine/threonine kinase activity, and endopeptidase activity (Fig. 2A). The signaling pathways identified by the KEGG pathway analysis were including the PI3K-AKT signaling pathway, TNF signaling pathway, NF- κ B signaling pathway, and so on (Fig. 2B).

3.3. Molecular docking and simulation

The PPI network and GO and KEGG pathway enrichment analyses revealed that LP treatment of influenza may entail the positive regulation of cytokine production, PI3K-AKT and TNF and NF- κ B signaling pathways. Notably, the transcription factor NF- κ B P65, known for its pivotal role in regulating the transcription of pro-inflammatory cytokines [31], is a central player in activating the TNF signaling pathway through the NF- κ B signaling pathway [32]. To delve deeper into these associations, we conducted molecular

Table 4
The top 10 high expression chemical compounds of LP.

Components	2DStructure	PubChem CID	Components	2DStructure	PubChem CID
L-Phenylalanine		6140	Isoleucine		6306
D-Phenylalanine		71567	L-Leucine		6106
HBOA		322636	Betaine		247
2-Phenylglycine		3866	Adenine		190
2-Hydroxy-6-aminopurine		76900	Adenosine		60961

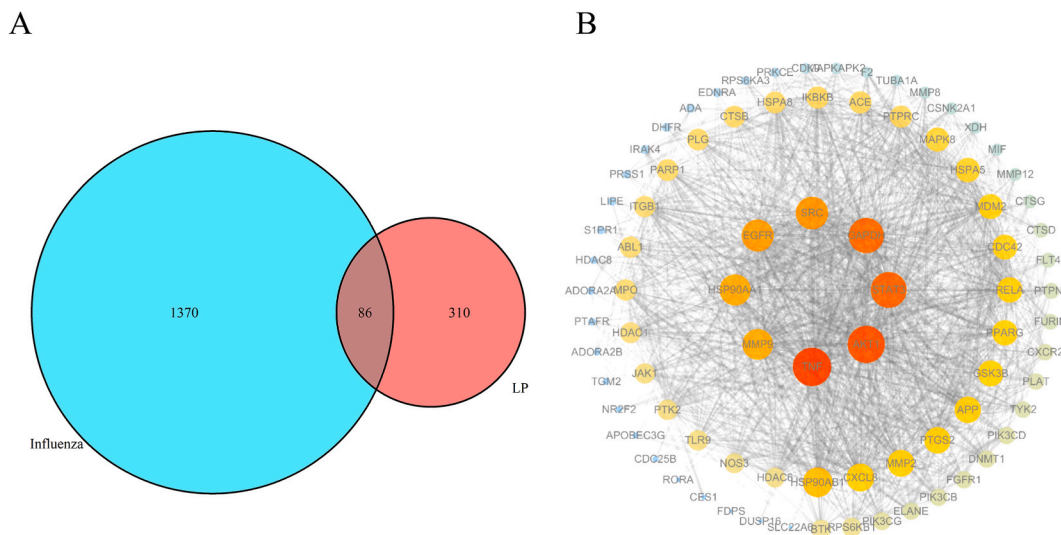


Fig. 1. (A) Venn diagram of the co-targets of influenza and LP. (B) PPI network of the co-targets of LP and influenza. Larger and darker nodes indicate a higher node degree value, suggesting a greater likelihood of exerting a vital function through the respective target.

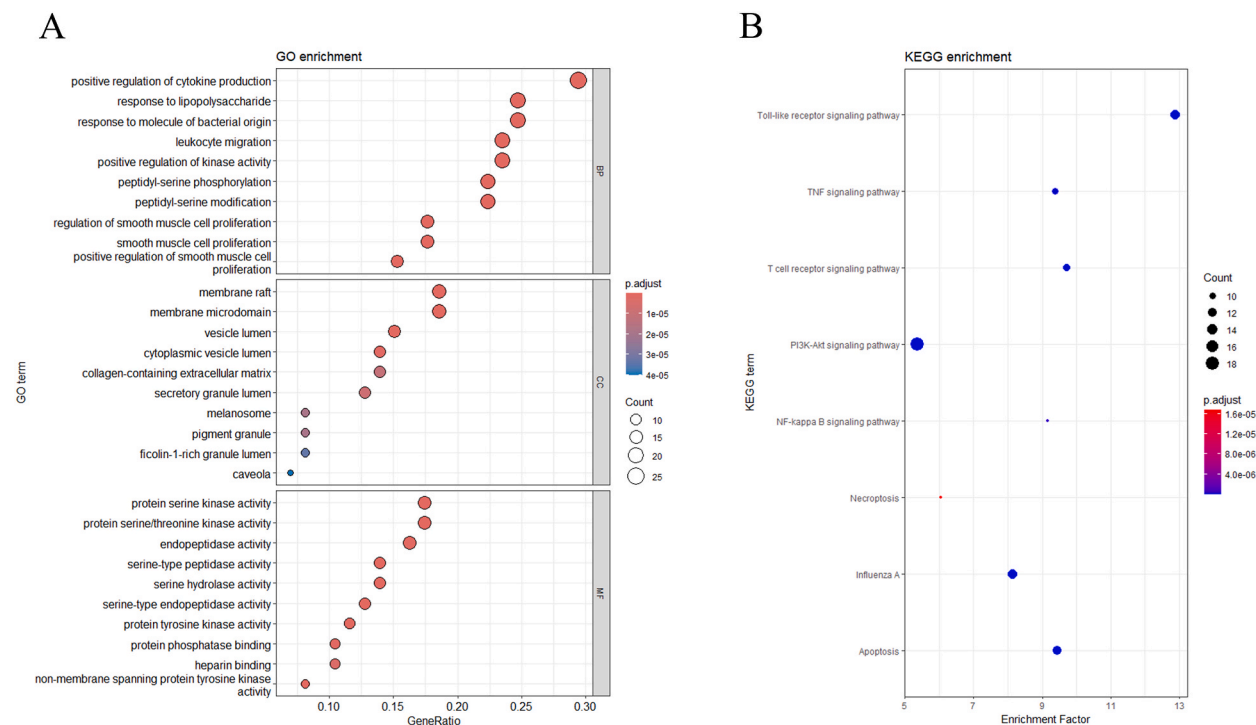


Fig. 2. Analysis of GO and KEGG enrichment to identify the anti-influenza mechanism of LP. (A) The top ten terms in biological processes (BP), cellular components (CC), and molecular functions (MF) that were highly enriched ($p < 0.05$) in the GO analysis were selected. (B) The pathways that were significantly enriched ($p < 0.05$) in KEGG analyses were selected.

docking to investigate the maximum binding energies of the compounds of LP with related proteins, including PI3K, AKT, TNF, and NF- κ B P65. In addition, amino acid [33] does not function as small ligand directly targeting the aforementioned proteins; therefore, we selected the remaining compounds from LP to perform molecular docking. In addition, the docking of the original ligands of the target protein was also performed for comparison. Table 5 provides an overview of the Autodock results. The original ligands demonstrated favorable binding energy with their respective receptors as anticipated and the binding energy of the original ligands except for the ligands of NF- κ B P65 was higher compared to the LP compounds interacting with these receptors. Our analysis revealed that the

affinity structure of the corresponding LP compounds bound to protein crystals fell within the range of 3–7 kcal/mol. Among the LP compounds, HBOA exhibited the lowest binding energy with PI3K, AKT, NF- κ B P65, and TNF with values of -3.83 , -6.92 , -5.9 , and -7.41 kcal/mol, respectively. While it is commonly accepted that a binding energy of < -5 kcal/mol is suggestive of substantial binding activity between a ligand and a receptor [34], our findings showed that the binding energy between PI3K and LP compounds exceeded -5 kcal/mol, suggesting that PI3K may not be the primary target for the theoretical impact that LP has on influenza. Molecular simulation revealed that the AKT-HBOA, NF- κ B-P65-HBOA, and TNF-HBOA complexes all maintained a stable interaction from 0 ns to 100 ns (Fig. 3A–C). TNF was the pro-inflammatory cytokine transcribed by NF- κ B, and AKT served as an upstream element in the regulation of NF- κ B activation [35,36]. Consequently, our speculation is that AKT/NF- κ B signaling pathway may constitute the key mediated pathway for influenza treatment with LP.

3.4. Molecular docking validation and comparison

To validate molecular docking, we performed re-docking of the crystallized ligands (CHEMBL213618 or 1-(4-methanoylphenyl)carbonylpiperidine-4-carbonitrile or [4-(isoquinolin-8-yl)phenyl]acetonitrile) to their respective proteins: AKT (2GU8), NF- κ B-P65 (7BIY), or TNF (6×81). The crystallized ligand was extracted from each protein and subsequently docked back into the same protein. The docking grid box was specifically constructed at the active site for each protein. To assess the accuracy of docking, we superimposed the lowest energy pose of the docked ligand onto the crystallized ligand, allowing us to calculate the RMSD. A successful validation of the docking process requires an RMSD of < 2 Å. As shown in Fig. 4A, D, G, the RMSD of the superimposed conformation of the docked and native ligands about CHEMBL213618, 1-(4-methanoylphenyl)carbonylpiperidine-4-carbonitrile, and [4-(isoquinolin-8-yl)phenyl]acetonitrile were 1.2475 Å, 1.6884 Å, and 0.8104 Å, respectively, which were all < 2 Å. Furthermore, molecular docking was conducted with the corresponding proteins for the AKT inhibitor (CHEMBL213618), NF- κ B-P65 inhibitor (magnolol), and TNF inhibitor (SPD304), revealing binding energy values of -10.0 , -6.27 , and -11.85 kcal/mol, respectively. As shown in Fig. 4 (B, C, E, F, H, I), 2D intermolecular interaction of the above complexes revealed that the compound HBOA had the same sites as the docked inhibitors of the target proteins produced. The results indicated that HBOA could be a potential molecular inhibitor that targets the AKT/NF- κ B signaling pathway.

3.5. LP improved the weight loss, decreased the lung index and virus titres, and reduced the number of lung lesions in mice post-infection

To assess the effectiveness of LP against H3N2, we monitored the daily body weight of mice for 6 days. As depicted in Fig. 5A, the H3N2 group exhibited a significant body weight loss of approximately 15 % compared with the Ctrl group. In contrast, the OSE, LP 1.2 g/kg, and LP 0.6 g/kg groups showed increased weight with an approximate increase of 5 %, 7 %, and 8 %, respectively, compared to the H3N2 group. Furthermore, to assess the severity of viral pneumonia induced by H3N2 (Fig. 5B), we calculated the lung index. The H3N2 group had a markedly higher lung index than the Ctrl group (1.09 ± 0.10 ; $p < 0.001$), whereas the OSE group had a significantly lower lung index than the H3N2 group (0.81 ± 0.07 ; $p < 0.001$); similar findings were noted for the LP 1.2 g/kg (0.87 ± 0.07 ; $p < 0.01$) and LP 0.6 g/kg (0.94 ± 0.07 ; $p < 0.05$) groups. Additionally, we determined the antiviral activity of LP by measuring the virus titres in the lungs. As shown in Fig. 5C, the virus titre in the H3N2 group was 5.70 ± 0.33 . Notably, both LP and OSE treatments significantly inhibited virus replication in the lungs of mice. The virus titres in the OSE, LP 1.2 g/kg, and LP 0.6 g/kg groups were 4.07 ± 0.35 ($p < 0.001$), 4.61 ± 0.20 ($p < 0.001$), and 4.90 ± 0.26 ($p < 0.001$), respectively.

Subsequently, we proceeded to examine histopathological changes in the lungs of the mice (Fig. 5D). Following infection with influenza virus, the alveoli of mice in the H3N2 group experienced extensive atrophy. Additionally, the alveolar walls exhibited thickening and dilation, accompanied by a significant infiltration of inflammatory cells within the alveoli. Conversely, when subjected to treatment with either OSE or LP, there was a marked improvement in alveolar atrophy, along with a noticeable decrease in the infiltration of inflammatory cells. These findings strongly revealed that LP has the ability to shield the host's lungs from damage inflicted by H3N2.

Table 5

The molecular docking's binding energy between the target proteins and LP compounds or the original ligands.

Protein Binding energy kcal/mol Compound	PI3K	AKT	TNF	NF- κ B-P65
HBOA	-3.83	-6.92	-5.95	-7.41
2-Hydroxy-6-aminopurine	-3.24	-6.03	-5.89	-6.97
Betaine	-2.85	-3.04	-3.61	-4.02
Adenine	-3.06	-5.64	-5.23	-5.66
Adenosine	-2.54	-6.87	-5.90	-6.32
RU-PYRIDOCARBAZOLE-2	-9.37	\	\	\
CHEMBL213618	\	-10.00	\	\
1-(4-methanoylphenyl)carbonylpiperidine-4-carbonitrile	\	\	\	-6.27
4-(isoquinolin-8-yl)phenyl]acetonitrile	\	\	-11.06	\

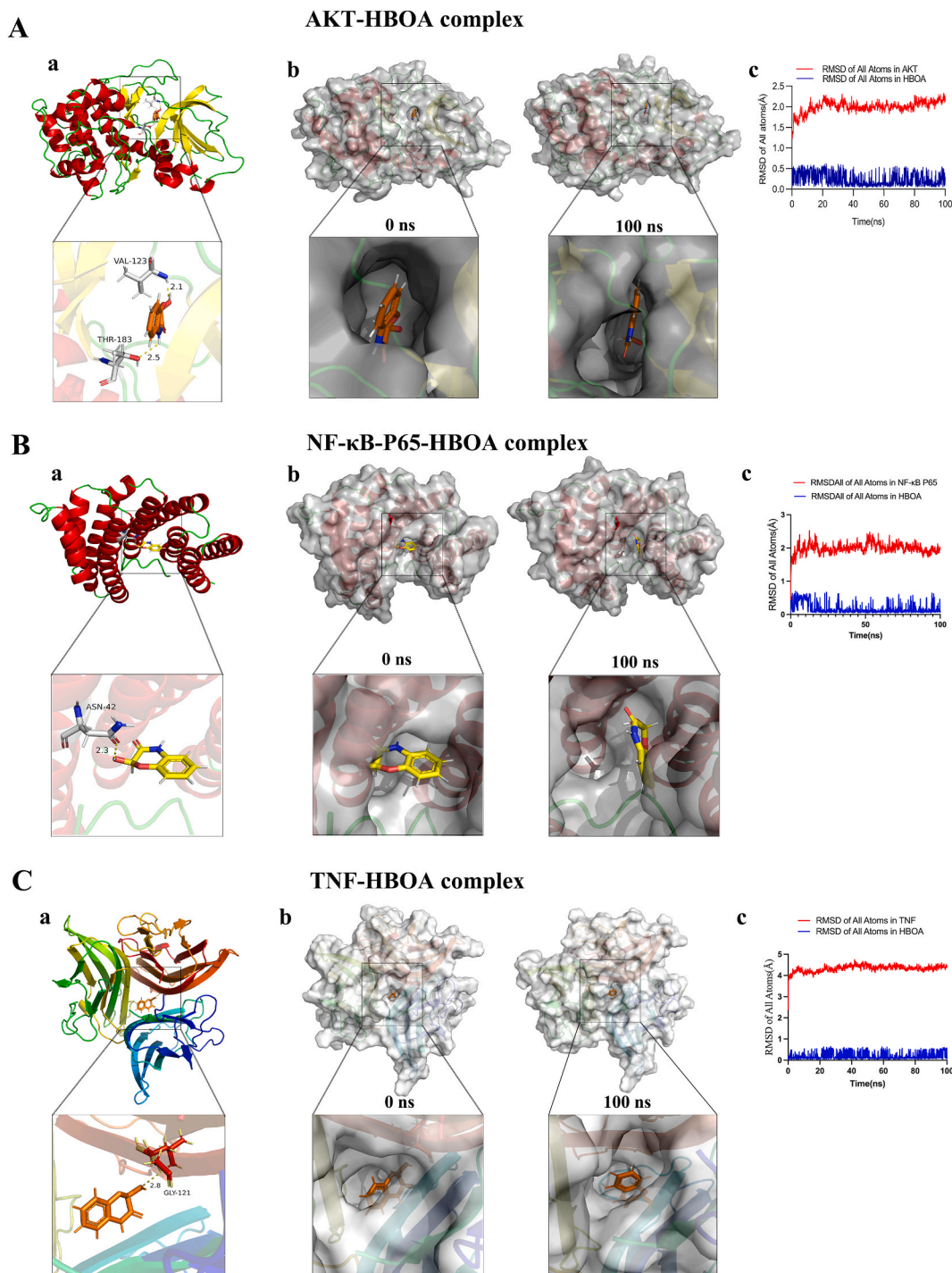


Fig. 3. Molecular docking and simulation of the compounds of LP and the target proteins. (A) AKT-HBOA complex: (a) Three-dimensional ribbon structure of the AKT-HBOA complex. (b) Surface simulation model of the AKT-HBOA complex in 0 and 100 ns. (c) RMSD of all atoms of AKT (red) and HBOA (blue). (B) The NF-κB-P65-HBOA complex: (a) Three-dimensional ribbon structure of the NF-κB-P65-HBOA. (b) Surface simulation model of the NF-κB-P65-HBOA complex in 0 and 100 ns. (c) RMSD of all atoms of NF-κB-P65 (red) and HBOA (blue). (C) The TNF-HBOA complex: (a) Three-dimensional ribbon structure of the TNF-HBOA complex. (b) Surface simulation model of the TNF-HBOA complex in 0 and 100 ns. (c) RMSD of all atoms of TNF (red) and HBOA (blue). (For interpretation of the references to colour in this figure legend, the reader is referred to the Web version of this article.)

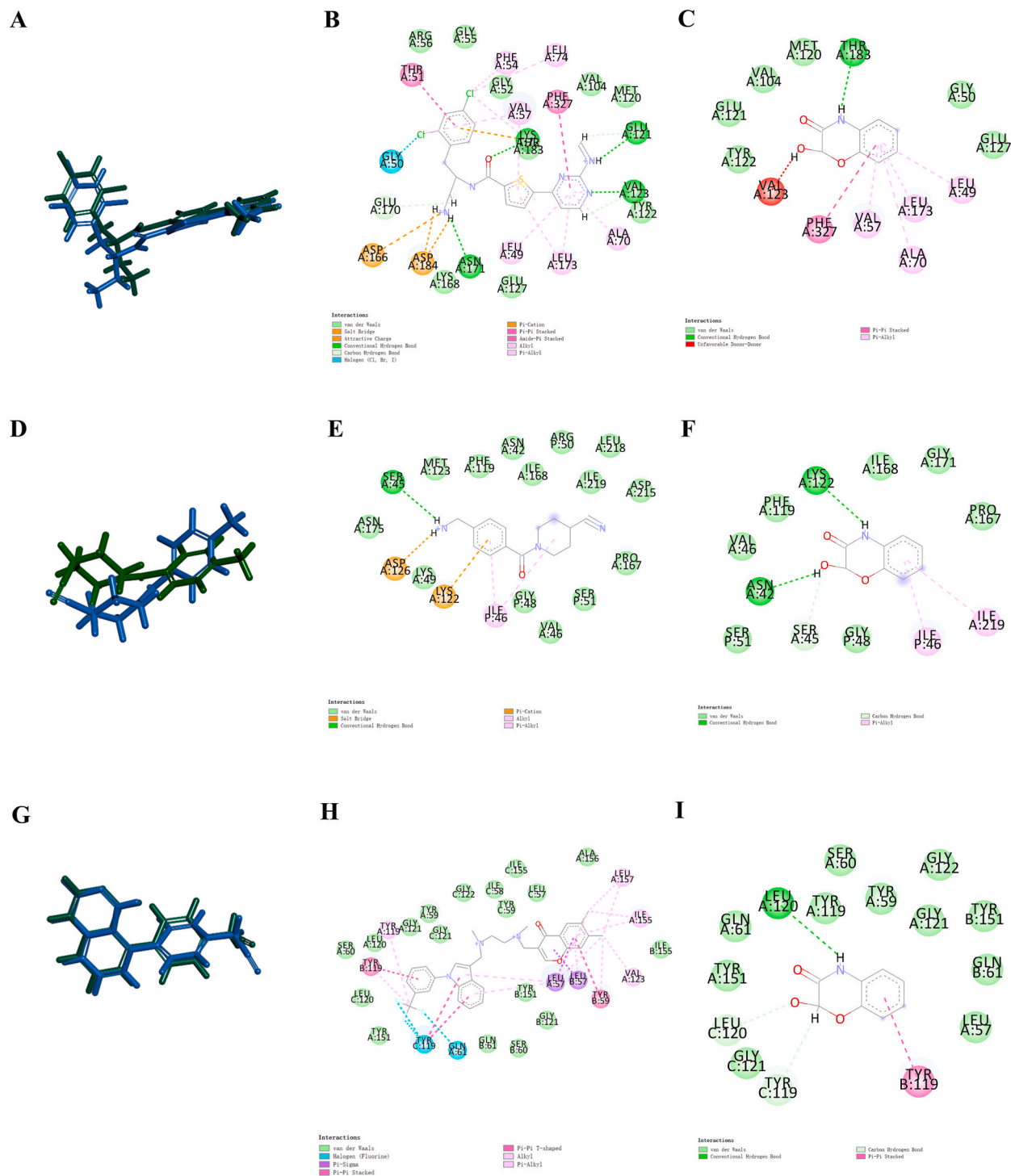


Fig. 4. Molecular docking validation and comparison. (A) Re-docking pose with RMSD value of 1.2475 Å (docked CHEMBL213618 presented in green and original CHEMBL213618 presented in blue). (B) 2D intermolecular interaction between CHEMBL213618 and AKT. (C) 2D intermolecular interaction between HBOA and AKT. (D) Re-docking pose with RMSD value of 1.6884 Å (docked 1-(4-methanoylphenyl)carbonylpiperidine-4-carbonitrile presented in green and original 1-(4-methanoylphenyl)carbonylpiperidine-4-carbonitrile presented in blue) (E) 2D intermolecular interaction between magnolol and NF-κB-P65. (F) 2D intermolecular interaction between HBOA and NF-κB-P65. (G) Re-docking pose with RMSD value of 0.8104 Å (docked [4-(isoquinolin-8-yl)phenyl]acetoneitrile presented in green and original [4-(isoquinolin-8-yl)phenyl]acetoneitrile presented in blue). (H) 2D intermolecular interaction between SPD304 and TNF. (I) 2D intermolecular interaction between HBOA and TNF. (For interpretation of the references to colour in this figure legend, the reader is referred to the Web version of this article.)

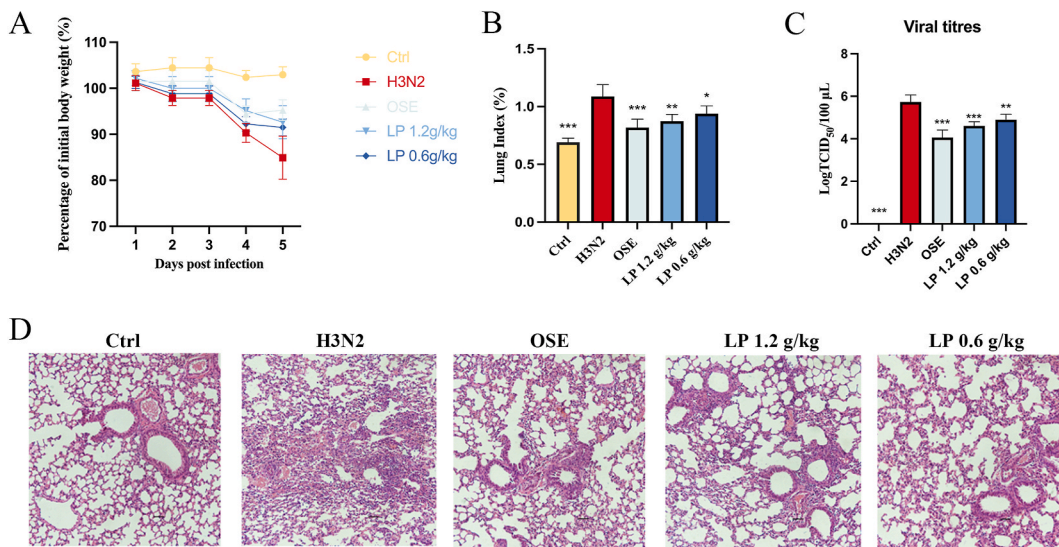


Fig. 5. Protective actions of LP on H3N2-infected mice. (A) Body weight changes in mice in the Ctrl group, the H3N2 group, the OSE group, the LP 1.2 g/kg group and the LP 0.6 g/kg group (the OSE and LP treatment from 4 h of H3N2 virus infection); (B) Alterations in the lung index of mice from each group; (C) Viral titers in the lungs of mice in each group; (D) HE staining of the pathological sections of the lungs in mice in each group after day 5 post-infection (magnification = 200×). The results are shown as mean \pm SD, * p < 0.05, ** p < 0.01, *** p < 0.001 vs. the H3N2 group.

3.6. Effect of LP on inflammation and immunity of lungs in mice post-infection

A regulated inflammatory response is crucial for clearing pathogens and safeguarding the host, but an excessive reaction can result in tissue damage and disrupt normal function. The overproduction of inflammatory cytokines can exacerbate this response. To assess these dynamics, qPCR was employed to measure the levels of pro-inflammatory cytokines in the lungs of mice after infection with H3N2. As illustrated in Fig. 6A, compared with the Ctrl group, the H3N2 group had significantly heightened mRNA expression levels of TNF- α , IL-6, IL-1 β , and MCP-1 (p < 0.001). Notably, compared with the H3N2 group, the LP 1.2 g/kg group had significantly reduced mRNA expression levels of TNF- α (p < 0.01), IL-6 (p < 0.01), IL-1 β (p < 0.05), and MCP-1 (p < 0.05), whereas the LP 0.6 g/kg group had significantly decreased levels of TNF- α (p < 0.01) and IL-6 (p < 0.01) but non-significant reductions in the levels of MCP-1 and IL-1 β . Furthermore, compared with the H3N2 group, the OSE group exhibited a significantly lower mRNA expression of the mentioned cytokines (p < 0.01 or p < 0.001).

Flow cytometry was utilized to assess the expression of T cells, specifically CD3⁺, CD4⁺, and CD8⁺, and to scrutinize changes in the immune response induced by H3N2 in the mouse lungs. CD3⁺, CD4⁺, and CD8⁺ T cells were significantly diminished in the H3N2 group compared with those in the Ctrl group (p < 0.01 or p < 0.05; Fig. 6B), whereas the LP 1.2 g/kg group showed no reduction in CD3⁺, CD4⁺, and CD8⁺ T cells (p < 0.05 or p < 0.01). The LP 0.6 g/kg group exhibited a slight, but non-significant, increase in these T cells compared with the H3N2 group. Furthermore, the OSE group demonstrated a substantial increase in the mentioned T cells (p < 0.01 or p < 0.05).

SDC-1 has immunomodulatory capabilities and is essential in controlling lung inflammation [37,38]. The respiratory mucosa, including plasma cells, tissue-resident memory B cells, and plasmablasts, secretes the antibody IgA [39]. IgA, in turn, binds to pIgR to form sIgA, which is then transported from the epithelium to neutralize the virus [40]. We conducted IHC to assess SDC-1 expression and employed ELISA to measure sIgA levels in the lungs. As depicted in Fig. 6C and D, compared with the Ctrl group, the H3N2 group exhibited significantly reduced SDC-1 and sIgA expressions (p < 0.01), whereas the LP 1.2 g/kg group showed markedly increased SDC-1 expression (p < 0.001) and elevated sIgA levels (p < 0.01) compared with the H3N2 group. On the other hand, the LP 0.6 g/kg group showed significantly increased SDC-1 expression (p < 0.01) compared with the H3N2 group. Notably, SDC-1 and sIgA expressions in the OSE group were not significantly increased compared with those in the H3N2 group. These results implied that LP treatment can mitigate excessive inflammation and enhance immunity in the lungs of mice infected with H3N2.

3.7. LP suppressed the phosphorylation of AKT and NF- κ B-P65 in the lungs of mice post-infection

Following H3N2 infection, we thoroughly examined the protein expression levels in the lungs of mice post LP administration, guided by the results from molecular docking and simulation studies. As depicted in Fig. 7A, B, a decrease in AKT expression was observed in the Ctrl, OSE, LP 1.2 g/kg, and LP 0.6 g/kg groups compared to the H3N2 group, although these variations did not reach statistical significance (p > 0.05). Conversely, there was a significant increase in the expression of p-AKT, NF- κ B-P65, and p-NF- κ B-P65 in the H3N2 group compared to the Ctrl group (p < 0.01 or p < 0.001). Notably, the expression of p-NF- κ B-P65 was significantly reduced in the LP 1.2 g/kg and LP 0.6 g/kg groups (p < 0.05) in comparison to the H3N2 group. Moreover, the LP 1.2 g/kg group

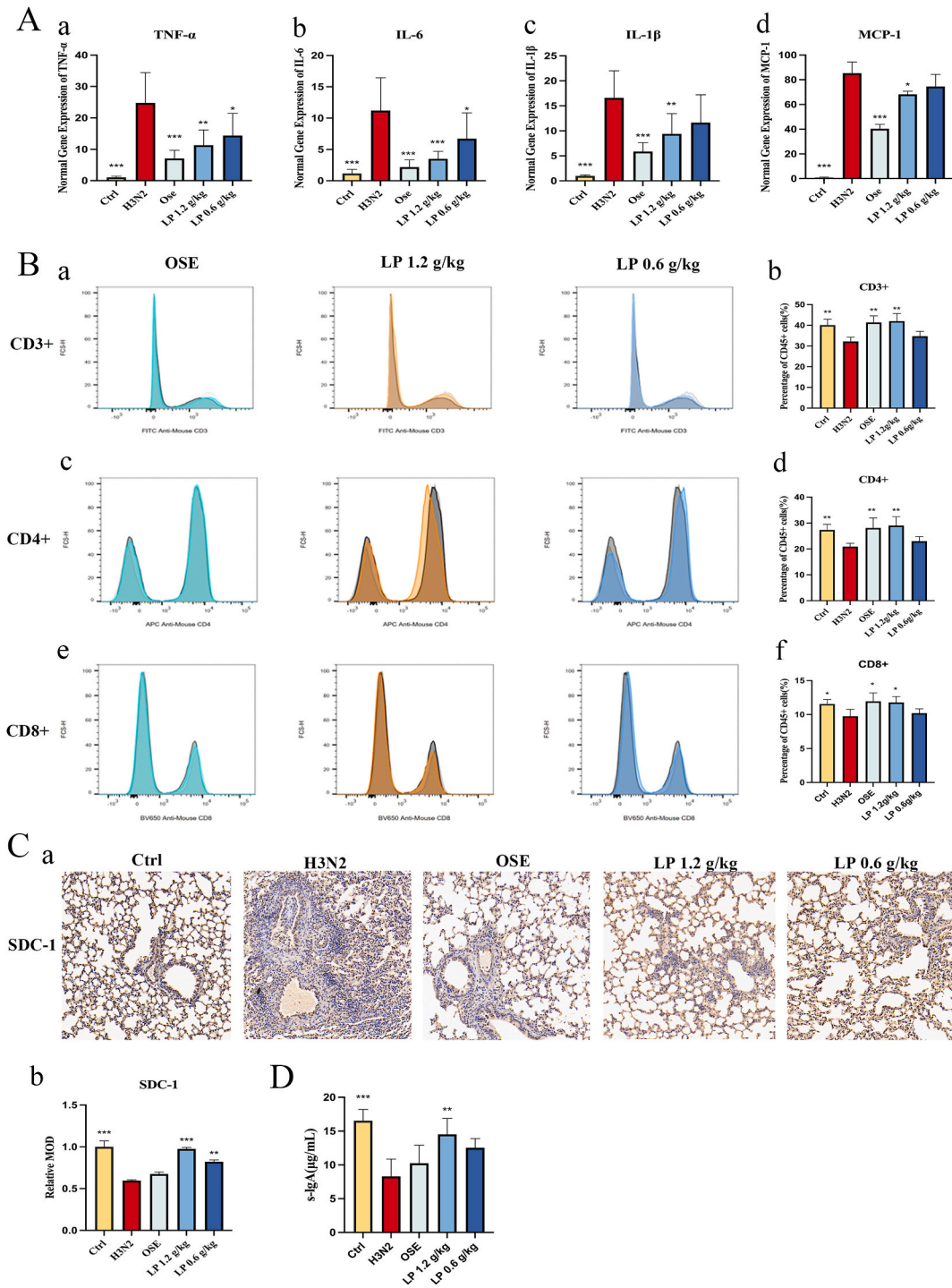


Fig. 6. Effects of LP treatment on inflammatory and immune response to H3N2 in the lungs of mice. (A) qPCR analysis of the mRNA expression of pro-inflammatory cytokines TNF- α , IL-6, IL-1 β , and MCP-1 in lungs of mice in the Ctrl group, the H3N2 group, the OSE group, the LP 1.2 g/kg group and the LP 0.6 g/kg group (the OSE and LP treatment from 4 h of H3N2 virus infection). (B) Flow cytometry analysis of T cells in lungs in each group, including CD3⁺, CD4⁺, and CD8⁺ T cells. (C) Immunohistochemistry assay detection of SDC-1 expression of lungs in each group (magnification = 400 \times). (D) ELISA detection of sIgA expression of lungs in each group. The results are shown as mean \pm SD, * p < 0.05, ** p < 0.01, *** p < 0.001 vs the H3N2 group.

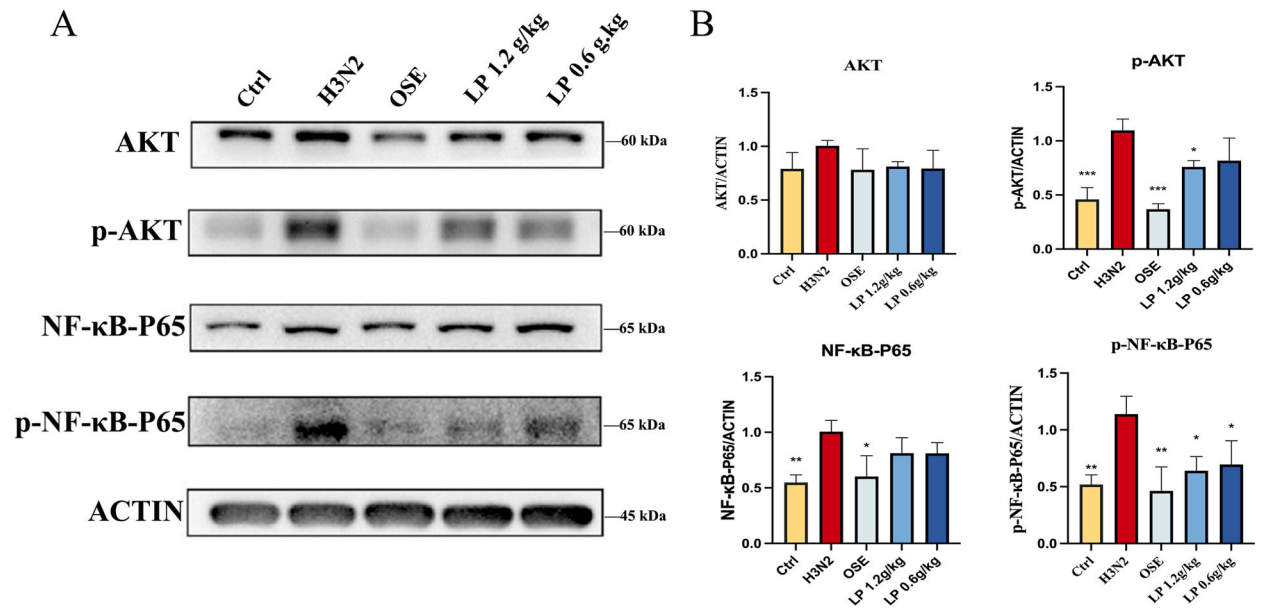


Fig. 7. Protein expression of AKT, *p*-AKT, NF- κ B-P65, and *p*-NF- κ B-P65. (A) Associated proteins (AKT, *p*-AKT, NF- κ B-P65, and *p*-NF- κ B-P65) in the lungs of mice in the Ctrl group, the H3N2 group, the OSE group, the LP 1.2 g/kg group and the LP 0.6 g/kg group (the OSE and LP treatment from 4 h of H3N2 virus infection) were detected using Western blot assay. (B) Quantification of the associated proteins (AKT, *p*-AKT, NF- κ B-P65, and *p*-NF- κ B-P65) was performed on Image J software. The results are presented as mean \pm SD, * p < 0.05, ** p < 0.01, *** p < 0.001 vs. the H3N2 group.

exhibited a significant decrease in *p*-AKT expression (p < 0.05), while the LP 0.6 g/kg group showed a non-significant decrease (p > 0.05). Additionally, the OSE group displayed markedly reduced protein levels of *p*-AKT, NF- κ B-P65, and *p*-NF- κ B-P65 (p < 0.001 or p < 0.01 or p < 0.05). These results suggest that LP therapy effectively inhibits the phosphorylation of AKT and NF- κ B-P65, offering protection against influenza-induced damage.

4. Discussion

In this study, we identified 1600 compounds in LP by employing LC-MS/MS analysis. Given the complex multi-component nature of LP, we carefully selected 10 main compounds and employed network pharmacology to comprehensively investigate possible mechanisms behind the effectiveness of LP in treating influenza. Network pharmacology represents a pioneering approach at the intersection of traditional Chinese medicine and modern science that has been widely adopted to elucidate the intricate interactions between drugs and diseases by examining holistic biological networks [41]. By combining the putative targets of LP with therapeutic targets associated with influenza virus infection, we identified 86 targets through network topological analysis. Subsequently, we performed PPI network and GO and KEGG enrichment analyses on these 86 targets, which revealed that LP might mitigate influenza virus infection by modulating pathways such as regulation of cytokine production, TNF, PI3K-AKT and NF- κ B signaling pathways. Importantly, the transcription factor NF- κ B P65, known for its role in regulating pro-inflammatory cytokine transcription [31], emerged as a key player in these mechanisms. Furthermore, we predicted that the target proteins responsible for the treatment of influenza virus infection with LP were TNF, PI3K, AKT, and NF- κ B P65. To validate these interactions, we employed molecular docking and dynamic simulation methods. Notably, our results demonstrated that HBOA formed better interactions with AKT, NF- κ B P65 and TNF compared to the other compounds of LP. Furthermore, upon comparing the intermolecular interaction sites of existing molecular inhibitors of these proteins with HBOA, we found that HBOA shares the same sites with these inhibitors. HBOA has previously demonstrated potential in blocking the NF- κ B signaling pathway to mitigate liver fibrosis [42]. Additionally, a literature review revealed the effects of other compounds in LP. For example, isoleucine, a branched-chain amino acid, is known to enhance the immune system, including both innate and adaptive immunity [43]. However, the specific effects of these compounds on influenza virus injury remain unclear. Thus, further studies should elucidate the impact and mechanisms of action of these compounds against influenza virus.

To elucidate the underlying mechanism, we conducted *in vivo* experiments to validate our network analysis findings. As demonstrated in the *in vivo* experiments, LP improved the weight loss of mice, decreased the lung index and viral titres, and alleviated pathological changes in the lungs induced by H3N2. Moreover, LP inhibited the release of TNF- α , IL-6, IL-1 β , and MCP-1 in the lungs of mice post-infection and prevented the depletion of CD3⁺, CD4⁺, and CD8⁺ T cells from the lungs of mice. Furthermore, LP exhibited inhibitory effects on the reduction of SDC-1 and sIgA expressions in the lungs of mice post-infection. The respiratory epithelial cell layer serves as the initial line of defense when the influenza virus enters the body through oral or nasal cavities. SDC-1 is an indicator of

intact respiratory epithelium and is essential in controlling innate immunity to mitigate lung injury and inflammation caused by influenza [38]. sIgA, the main antibody in mucus, provides non-specific protection by neutralizing viruses and other pathogens [44]. Changes in SDC-1 and sIgA levels reflect immune responses at mucosal surfaces to combat influenza virus invasion. Pro-inflammatory cytokines and chemokines are released as the virus replicates in host cells and activates various pattern recognition receptors. Excessive pro-inflammatory cytokine production exacerbates inflammation, cell death, and the release of progeny viruses [45]. In addition, chemokines recruit additional immune cells. T cells are essential in antiviral immune response [46]. CD3, composed of three polypeptides, is expressed in all T cells [47]; therefore, CD3⁺ T cells can serve as an active marker total T cells. While CD8⁺ T cells release cytotoxic particles to destroy infected cells, CD4⁺ T cells emit a variety of cytokines that support the development of protective antibodies [48]. The number of lymphocytes typically decreases in influenza-infected patients [49]. Additionally, the susceptibility to H3N2 could be reduced by augmenting CD4⁺ and CD8⁺ T cells [49]. However, following H3N2 infection, LP treatment appears to restore host immunity, reduce excessive inflammation, and restrict viral reproduction and spread, indicating the potential anti-influenza therapeutic mechanisms of LP.

As the limitation of the study, we didn't perform internal validation of LC-MS/MS analysis and further explore mechanism of the individual compound of LP on inflammation and immunity against H3N2. In addition, we selected only the first ten major monomer compounds (excluding some uncertain ones) for network pharmacology analysis. The potential mechanism of action of the other monomer compounds in LP remains deserving of further investigation.

Furthermore, the results from network analysis, molecular docking, and simulation demonstrated that AKT and NF- κ B P65 are the core potential targets for LP treatment of influenza. This hypothesis gains support from Western blot assays, which confirm that LP can inhibit the phosphorylation of these proteins. AKT, a serine-threonine kinase, is essential for several functions, including cell division, metabolism, and proliferation [50]. AKT interacts with the non-structural protein 1 (NS1) of the influenza virus, and its activity may reduce the sensitivity of conventional T cells, ultimately promoting susceptibility to influenza virus infection [51–53]. Furthermore, AKT is a crucial upstream element that regulates NF- κ B activation [35], while NF- κ B itself is vital in regulating immune development, immune reaction, inflammation, and various cellular activities [54]. Notably, when the NF- κ B pathway is activated, it induces the release of the aforementioned cytokines [31]. Taken together, the mechanism of action of LP against H3N2 involves inhibiting the AKT/NF- κ B signaling pathway, which, in turn, helps restore physiological homeostasis in the host.

5. Conclusion

To sum up, our study demonstrates that LP has the capability to boost host immunity and curb the excessive production of pro-inflammatory cytokines, thereby shielding the host from H3N2 infection. The mechanism of action of LP against influenza virus involves inhibiting the AKT/NF- κ B signaling pathway. These results establish a theoretical and research groundwork for considering LP and its components as a potential countermeasure against influenza.

Date availability statement

Data will be made available on request.

CRediT authorship contribution statement

Yaorong Chen: Writing – original draft, Validation, Methodology, Formal analysis, Data curation. **Zexing Chen:** Writing – original draft, Validation, Formal analysis, Data curation. **Wanqi Wang:** Methodology, Investigation, Data curation. **Yutao Wang:** Supervision, Data curation. **Jinyi Zhu:** Methodology, Data curation. **Xinhua Wang:** Project administration, Funding acquisition. **Wanyi Huang:** Writing – review & editing, Project administration, Funding acquisition.

Declaration of competing interest

The authors declare that they have no known competing financial interests or personal relationships that could have appeared to influence the work reported in this paper.

Acknowledgements

This study was supported by the National Natural Science Foundation of China (Grant No. 8190140129) and the National Famous Old Chinese Medicine Experts Inheritance Studio Construction Project, under the National Chinese Medicine Human Education Letter [2022] No. 75.

Appendix A. Supplementary data

Supplementary data to this article can be found online at <https://doi.org/10.1016/j.heliyon.2024.e29487>.

References

- [1] K. F. S. Gjd, F. Ram, P. M, K. K, D. Pc, P. P, S. Ml, T. J, W. Rg, G.-S. A, Influenza, Nat. Rev. Dis. Prim. 4 (2018), <https://doi.org/10.1038/s41572-018-0002-y>.
- [2] K. Ac, T. Pg, Influenza virus-related critical illness: pathophysiology and epidemiology, Crit. Care 23 (2019), <https://doi.org/10.1186/s13054-019-2539-x>.
- [3] R.A. Medina, 1918 influenza virus: 100 years on, are we prepared against the next influenza pandemic? Nat. Rev. Microbiol. 16 (2018) 61, <https://doi.org/10.1038/nrmicro.2017.174>.
- [4] S. Jm, S. N, S. W, M. A, Evolution of influenza viruses-drug resistance, treatment options, and prospects, Int. J. Mol. Sci. 23 (2022), <https://doi.org/10.3390/ijms232012244>.
- [5] J. Jc, Y. Hl, A. P, A. K, G. Ea, Influenza antivirals and their role in pandemic preparedness, Antivir. Res. 210 (2023), <https://doi.org/10.1016/j.antiviral.2022.105499>.
- [6] P. Ci, F. As, Influenza vaccines: good, but we can do better, J. Infect. Dis. 219 (2019), <https://doi.org/10.1093/infdis/jiy633>.
- [7] MdM. Rahman, S. Bibi, MdS. Rahaman, F. Rahman, F. Islam, M.S. Khan, M.M. Hasan, A. Parvez, MdA. Hossain, S.K. Maeesa, MdR. Islam, A. Najda, H.S. Al-malky, H.R.H. Mohamed, H.I.M. AlGwaiz, A.A. Awaji, M.O. Germoush, O.A. Kensara, M.M. Abdel-Daim, M. Saeed, M.A. Kamal, Natural therapeutics and nutraceuticals for lung diseases: traditional significance, phytochemistry, and pharmacology, Biomed. Pharmacother. 150 (2022) 113041, <https://doi.org/10.1016/j.biopha.2022.113041>.
- [8] L. H, Y. L, W. J, Z. M, G. R, Z. H, S. R, M. Q, D. D, H. Y, Berberine suppresses influenza virus-triggered NLRP3 inflammasome activation in macrophages by inducing mitophagy and decreasing mitochondrial ROS, J. Leukoc. Biol. 108 (2020), <https://doi.org/10.1002/JLB.3MA0320-358RR>.
- [9] Y. W, Z. M, X. P, L. J, W. H, Effect of paeoniflorin on acute lung injury induced by influenza A virus in mice, Evidences of its mechanism of action, Phytomedicine : International Journal of Phytotherapy and Phytomedicine 92 (2021), <https://doi.org/10.1016/j.phymed.2021.153724>.
- [10] S. X, L. T, S. P, X. X, H. P, C. H, M. E, Efficacy and safety of Lagergera pterodonta in children 3-24 months with acute bronchiolitis: a randomized controlled trial, The Clinical Respiratory Journal 11 (2017), <https://doi.org/10.1111/crj.12334>.
- [11] W. Y, Y. L, W. F, W. X, Z. C, S. S, M. J, Z. Y, Hepatoprotective and antioxidative effects of total phenolics from Lagergera pterodonta on chemical-induced injury in primary cultured neonatal rat hepatocytes, Food Chem. Toxicol. : An International Journal Published for the British Industrial Biological Research Association 45 (2007), <https://doi.org/10.1016/j.fct.2007.01.011>.
- [12] L. J, L. F, W. G, G. F, L. H, X. L, H. X, Z. Y, D. X, Q. X, Acetylcholinesterase inhibitory activity of sesquiterpenoids isolated from Lagergera pterodonta, Front. Plant Sci. 14 (2023), <https://doi.org/10.3389/fpls.2023.1074184>.
- [13] W. Y, L. J, Y. W, C. Q, J. Z, Z. R, P. X, W. X, An active component containing pterodonic acid and pterodondiol isolated from Lagergera pterodonta inhibits influenza A virus infection through the TLR7/MyD88/TRAF6/NF- κ B signaling pathway, Mol. Med. Rep. 18 (2018), <https://doi.org/10.3892/mmr.2018.8947>.
- [14] W. Guan, J. Li, Q. Chen, Z. Jiang, R. Zhang, X. Wang, Z. Yang, X. Pan, Pterodonic acid isolated from Lagergera pterodonta inhibits viral replication and inflammation induced by influenza A virus, Molecules 22 (2017) 1738, <https://doi.org/10.3390/molecules22101738>.
- [15] X. Wang, Y. Liu, N. Kang, G. Xu, Wide identification of chemical constituents in fermented licorice and explore its efficacy of anti-neurodegeneration by combining quasi-targeted metabolomics and in-depth bioinformatics, Front. Neurosci. 17 (2023) 1156037, <https://doi.org/10.3389/fnins.2023.1156037>.
- [16] N. C, M. Zm, L. M, K. C, C. Ai, S. Hhhw, Network pharmacology: curing causal mechanisms instead of treating symptoms, Trends Pharmacol. Sci. 43 (2022), <https://doi.org/10.1016/j.tips.2021.11.004>.
- [17] M. Xy, Z. Hx, M. M, C. M, Molecular docking: a powerful approach for structure-based drug discovery, Curr. Comput. Aided Drug Des. 7 (2011), <https://doi.org/10.2174/157340911795677602>.
- [18] Z. Yang, J. Man, Y. Liu, H. Zhang, D. Wu, D. Shao, B. Hao, S. Wang, Study on the alleviating effect and potential mechanism of ethanolic extract of limonium aureum (L.) hill. On lipopolysaccharide-induced inflammatory responses in macrophages, Indian J. Manag. Sci. 24 (2023) 16272, <https://doi.org/10.3390/ijms242216272>.
- [19] The Human Serum Metabolome (HUSERMET) Consortium, W.B. Dunn, D. Broadhurst, P. Begley, E. Zelena, S. Francis-McIntyre, N. Anderson, M. Brown, J. D. Knowles, A. Halsall, J.N. Haselden, A.W. Nicholls, I.D. Wilson, D.B. Kell, R. Goodacre, Procedures for large-scale metabolic profiling of serum and plasma using gas chromatography and liquid chromatography coupled to mass spectrometry, Nat. Protoc. 6 (2011) 1060–1083, <https://doi.org/10.1038/nprot.2011.335>.
- [20] E.J. Want, I.D. Wilson, H. Gika, G. Theodoridis, R.S. Plumb, J. Shockcor, E. Holmes, J.K. Nicholson, Global metabolic profiling procedures for urine using UPLC-MS, Nat. Protoc. 5 (2010) 1005–1018, <https://doi.org/10.1038/nprot.2010.50>.
- [21] M. Gm, H. R, L. W, S. Mf, B. Rk, G. Ds, O. Aj, AutoDock 4 and AutoDockTools 4: automated docking with selective receptor flexibility, J. Comput. Chem. 30 (2009), <https://doi.org/10.1002/jcc.21256>.
- [22] K. M, T. A, van der L. A. E, G, Structural, Hirshfeld surface and molecular docking studies of a new organotin(IV)-phosphoric triamide complex and an amidophosphoric acid ester proposed as possible SARS-CoV-2 and Monkeypox inhibitors, Heliyon 9 (2023) e17358, <https://doi.org/10.1016/j.heliyon.2023.e17358>.
- [23] M. Ja, M. C, K. K, W. L, H. Ke, S. C, ff14SB: improving the accuracy of protein side chain and backbone parameters from ff99SB, J. Chem. Theor. Comput. 11 (2015), <https://doi.org/10.1021/acs.jctc.5b00255>.
- [24] H. Mf, D. B, Structure and dynamics of TIP3P, TIP4P, and TIP5P water near smooth and atomistic walls of different hydroaffinity, J. Chem. Phys. 140 (2014), <https://doi.org/10.1063/1.4872239>.
- [25] K. E, V. G, New ways to boost molecular dynamics simulations, J. Comput. Chem. 36 (2015), <https://doi.org/10.1002/jcc.23899>.
- [26] OECD/OCDE, OECD guidelines for the testing of chemicals -acute oral toxicity – up-and-down-procedure (UDP). 425 - adopted: 3 October 2008. <https://www.oecd-ilibrary.org/content/publication/9789264071049-en>, 2019.
- [27] H.-J. Zhi, H.-Y. Zhu, Y.-Y. Zhang, Y. Lu, H. Li, D.-F. Chen, In vivo effect of quantified flavonoids-enriched extract of Scutellaria baicalensis root on acute lung injury induced by influenza A virus, Phytomedicine 57 (2019) 105–116, <https://doi.org/10.1016/j.phymed.2018.12.009>.
- [28] Q. Ma, B. Lei, R. Chen, B. Liu, W. Lu, H. Jiang, Z. Chen, X. Guo, Y. Wang, L. Zhang, Q. Chen, X. Li, Z. Yang, Liushen Capsules, a promising clinical candidate for COVID-19, alleviates SARS-CoV-2-induced pulmonary in vivo and inhibits the proliferation of the variant virus strains in vitro, Chin. Med. 17 (2022) 40, <https://doi.org/10.1186/s13020-022-00598-4>.
- [29] H.-X. Zhou, R.-F. Li, Y.-F. Wang, L.-H. Shen, L.-H. Cai, Y.-C. Weng, H.-R. Zhang, X.-X. Chen, X. Wu, R.-F. Chen, H.-M. Jiang, C. Wang, M. Yang, J. Lu, X.-D. Luo, Z. Jiang, Z.-F. Yang, Total alkaloids from Alstonia scholaris inhibit influenza A virus replication and lung immunopathology by regulating the innate immune response, Phytomedicine 77 (2020) 153272, <https://doi.org/10.1016/j.phymed.2020.153272>.
- [30] C. Zhang, Y. Zhao, X. Yang, Azilsartan attenuates lipopolysaccharide-induced acute lung injury via the Nrf 2/HO-1 signaling pathway, Immunol. Res. 70 (2022) 97–105, <https://doi.org/10.1007/s12026-021-09240-1>.
- [31] Y. Shi, H. Xu, Y. Xiao, P. Liu, P. Pang, S. Wu, L. Deng, X. Chen, Gegen qinlian decoction downregulates the TLR7 signalling pathway to control influenza A virus infection, Biomed. Pharmacother. 121 (2020) 109471, <https://doi.org/10.1016/j.biopha.2019.109471>.
- [32] D. Zhang, H. Li, X. Luo, D. Liu, Q. Wei, X. Ye, Integrated 16S rDNA, metabolomics, and TNF- α /NF- κ B signaling pathway analyses to explain the modulatory effect of Poria cocos aqueous extract on anxiety-like behavior, Phytomedicine 104 (2022) 154300, <https://doi.org/10.1016/j.phymed.2022.154300>.
- [33] K. B, P. El, Amino assets: how amino acids support immunity, Cell Metabol. 32 (2020), <https://doi.org/10.1016/j.cmet.2020.06.010>.
- [34] L. X, W. S, N. S, M. X, L. H, J. M, Z. Y, Network pharmacology prediction and molecular docking-based strategy to explore the potential mechanism of Huanglian Jiedu Decoction against sepsis, Comput. Biol. Med. 144 (2022), <https://doi.org/10.1016/j.combiomed.2022.105389>.
- [35] B. S, C. R, N. D, J. P, A. A, G. B, Regulation of NF- κ B activation through a novel PI-3K-independent and PKA/Akt-dependent pathway in human umbilical vein endothelial cells, PLoS One 7 (2012), <https://doi.org/10.1371/journal.pone.0046528>.
- [36] G. van Loo, M.J.M. Bertrand, Death by TNF: a road to inflammation, Nat. Rev. Immunol. 23 (2023) 289, <https://doi.org/10.1038/s41577-022-00792-3>.
- [37] M. Kouwenberg, A. Rops, M.B. Beber, L. Diepeveen, M. Götte, L. Hilbrands, J. van der Vlag, Role of syndecan-1 in the interaction between dendritic cells and T cells, PLoS One 15 (2020), <https://doi.org/10.1371/journal.pone.0230835>.

- [38] R. Brauer, L. Ge, S.Y. Schlesinger, T.P. Birkland, Y. Huang, T. Parimon, V. Lee, B.L. McKinney, J.K. McGuire, W.C. Parks, P. Chen, Syndecan-1 attenuates lung injury during influenza infection by potentiating c-met signaling to suppress epithelial apoptosis, *Am. J. Respir. Crit. Care Med.* 194 (2016) 333–344, <https://doi.org/10.1164/rccm.201509-1878OC>.
- [39] O. Je, S. E. M. M, W. P, Z. S, J. R, S. S, K. Sh, K. F, I. A, Intranasal priming induces local lung-resident B cell populations that secrete protective mucosal antiviral IgA, *Science Immunology* 6 (2021), <https://doi.org/10.1126/sciimmunol.abj5129>.
- [40] W. Y, W. G, L. Y, Z. Q, S. H, G. N, X. J, Structural insights into secretory immunoglobulin A and its interaction with a pneumococcal adhesin, *Cell Res.* 30 (2020), <https://doi.org/10.1016/j.phrs.2023.106682>.
- [41] C. M, Z. G, L. M, H. H, Z. J, C. J, Z. M, L. Q, T. G, L. J, Z. H, Integrating network analysis and experimental validation to reveal the mitophagy-associated mechanism of Yiqi Huoxue (YQH) prescription in the treatment of myocardial ischemia/reperfusion injury, *Pharmacol. Res.* 189 (2023), <https://doi.org/10.1016/j.phrs.2023.106682>.
- [42] X. Sun, X. Huang, X. Zhu, L. Liu, S. Mo, H. Wang, X. Wei, S. Lu, F. Bai, D. Wang, X. Lin, J. Lin, HBOA ameliorates CCl4-induced liver fibrosis through inhibiting TGF- β 1/Smads, NF- κ B and ERK signaling pathways, *Biomed. Pharmacother.* 115 (2019) 108901, <https://doi.org/10.1016/j.biopha.2019.108901>.
- [43] G. C, M. X, C. D, Y. B, Y. Q, Isoleucine plays an important role for maintaining immune function, *Curr. Protein Pept. Sci.* 20 (2019), <https://doi.org/10.2174/1389203720666190305163135>.
- [44] Z. H, A. S, K. H, V. J, Respiratory antiviral immunity and immunobiotics: beneficial effects on inflammation-coagulation interaction during influenza virus infection, *Front. Immunol.* 7 (2016), <https://doi.org/10.3389/fimmu.2016.00633>.
- [45] S. Bedoui, M.J. Herold, A. Strasser, Emerging connectivity of programmed cell death pathways and its physiological implications, *Nat. Rev. Mol. Cell Biol.* 21 (2020) 678–695, <https://doi.org/10.1038/s41580-020-0270-8>.
- [46] T.J. Braciale, J. Sun, T.S. Kim, Regulating the adaptive immune response to respiratory virus infection, *Nat. Rev. Immunol.* 12 (2012) 295–305, <https://doi.org/10.1038/nri3166>.
- [47] A. A, A. B, D.B. V, Cell biology of T cell receptor expression and regulation, *Annu. Rev. Immunol.* 36 (2018), <https://doi.org/10.1146/annurev-immunol-042617-053429>.
- [48] Y. J, L. H, J. J, H. Z, L. S, Z. Y, M. S, D. X, Z. X, W. Y, S. X, C. D, H. L, F. X, L. Wj, C. B, Pandemic influenza A (H1N1) virus causes abortive infection of primary human T cells, *Emerg. Microb. Infect.* 11 (2022), <https://doi.org/10.1080/22221751.2022.2056523>.
- [49] T. Tk, L. Kt, L. Y, F. Vj, M. X, L. Nhl, P. Jsm, L. Gm, C. Bj, T. W, Investigation of CD4 and CD8 T cell-mediated protection against influenza A virus in a cohort study, *BMC Med.* 20 (2022), <https://doi.org/10.1186/s12916-022-02429-7>.
- [50] M. Guerau-de-Arellano, Z.L. Piedra-Quintero, P.N. Tschlis, Akt isoforms in the immune system, *Front. Immunol.* 13 (2022) 990874, <https://doi.org/10.3389/fimmu.2022.990874>.
- [51] K. Cg, K. T, C. Pj, K. T, Y. K, K. Gk, C. E, H. Sp, W. Pt, T. La, C. Y, TRAF6 is a T cell-intrinsic negative regulator required for the maintenance of immune homeostasis, *Nat. Med.* 12 (2006), <https://doi.org/10.1038/nm1449>.
- [52] H. N, S. F, M.-L. M, E. T, B. J, N. M, Inhibition of Akt kinase activity suppresses entry and replication of influenza virus, *Biochem. Biophys. Res. Commun.* 450 (2014), <https://doi.org/10.1016/j.bbrc.2014.06.077>.
- [53] J.-R. Jheng, C.-F. Hsieh, Y.-H. Chang, J.-Y. Ho, W.-F. Tang, Z.-Y. Chen, C.-J. Liu, T.-J. Lin, L.-Y. Huang, J.-H. Chern, J.-T. Horng, Rosmarinic acid interferes with influenza virus A entry and replication by decreasing GSK3 β and phosphorylated AKT expression levels, *J. Microbiol. Immunol. Infect.* 55 (2022) 598–610, <https://doi.org/10.1016/j.jmii.2022.04.012>.
- [54] M. S, V. J, H. A, Signaling via the NF κ B system, *wiley interdisciplinary reviews, Systems Biology and Medicine* 8 (2016), <https://doi.org/10.1002/wsbm.1331>.